Protection against ulcerative colitis and colorectal cancer by evodiamine via anti-inflammatory effects

YONGFENG ZHANG[1*], YAQIN ZHANG[1*], YANG ZHAO[2*], WANYUE WU[1], WEIQI MENG[1], YULIN ZHOU[1], YE QIU[3] and CHENLIANG LI[1]

[1]School of Life Sciences; [2]Department of Pharmacy, Jilin University, Changchun, Jilin 130021; [3]Department of Pharmacy, Changchun University of Chinese Medicine, Changchun, Jilin 130119, P.R. China

Received November 16, 2021; Accepted February 15, 2022

DOI: 10.3892/mmr.2022.12704

Abstract. Evodiamine (Evo) is an alkaloid that can be extracted from the berry fruit *Evodia rutaecarpa* and has been reported to exert various pharmacological effects, such as antidiarrheal, antiemetic and antiulcer effects. *In vivo*, the potential effects of Evo were investigated in a mouse model of dextran sodium sulfate (DSS)-induced ulcerative colitis (UC) and in adenomatous polyposis coli (Apc)^{MinC}/Gpt C57BL/6 mice with colorectal cancer (CRC), where the latter harbours a point-mutation in the *Apc* gene. Evo suppressed the degree of weight loss and colon shortening induced by DSS, decreased the disease activity index value and ameliorated the pathological alterations in the colon of mice with UC as examined via H&E staining of colon tissues. In addition, Evo decreased the number and size of colonic tumors in Apc^{MinC}/Gpt mice. Proteomics (colon tissues), ELISA (colon tissues and serum) and western blotting (colon tissues) results revealed that Evo inhibited NF-κB to mediate the levels of various cytokines, including, in the DSS-induced UC model, IL-1β, IL-2, IL-6, IL-8, TNF-α, IFN-γ (ELISA of colon tissues and serum), NF-κB, IKKα+β, IκBα, S100a9, TLR4 and MyD88 (western blotting of colon tissues), and, in the colorectal cancer model, IL-1β, IL-2, IL-6, IL-15, IL-17, IL-22, TNF-α (ELISA of colon tissues and serum), NF-κB, IKKα+β, IκBα and S100a9 (western blotting of colon tissues), to achieve its anti-inflammatory and antitumor effects. *In vitro*, Evo also reduced the viability of the colon cancer cell line SW480, inhibited mitochondrial membrane potential (MMP detection), caused G_2/M-phase arrest (cell cycle detection) and suppressed the translocation of phosphorylated-NF-κB from the cytoplasm into the nucleus (immunofluorescence of p-NF-κB). Theoretical evidence (MD simulations) suggest that Evo may bind to the ordered domain (α-helix) of NF-κB to influence this protein. The protein secondary structure changes were analyzed by the cpptraj module in Amber. In addition, these data provide experimental evidence that Evo may be an effective agent for treating UC and CRC.

Correspondence to: Dr Ye Qiu, Department of Pharmacy, Changchun University of Chinese Medicine, 1035 Boshuo Road, Changchun, Jilin 130119, P.R. China
E-mail: ccyeqiu@163.com

Mr. Chenliang Li, School of Life Sciences, Jilin University, 2699 Qianjin Street, Changchun, Jilin 130021, P.R. China
E-mail: lichenliang@jlu.edu.cn

*Contributed equally

Abbreviations: APC, adenomatous polyposis coli; CRC, colorectal cancer; DAI, disease activity index; DSS, dextran sodium sulfate; Evo, Evodiamine; GO, Gene Ontology; IBD, Inflammatory bowel disease; IKKα+β, inhibitor of NF-κB kinase α+β; KEGG, Kyoto Encyclopedia of Genes and Genomes; MD, molecular dynamics; MMP, mitochondrial membrane potential; MyD88, myeloid differentiation factor 88; SASP, Sulfasalazine; TLR4, Toll-like receptor 4; UC, ulcerative colitis

Key words: evodiamine, ulcerative colitis, colorectal cancer, inflammation, NF-κB

Introduction

Inflammatory bowel disease (IBD) is a group of chronic diseases in the digestive system that includes ulcerative colitis (UC) and Crohn's disease (CD) (1). It is empirically diagnosed based on endoscopic, pathological, clinical and radiological characteristics (2), but the pathogenesis of IBD remains unclear. UC is characterized by pathological damage in the mucosal layer and colonic ulceration (3), and CD is characterized by intraabdominal abscesses, fistulas and perianal disease (4). Colorectal cancer (CRC) is one of the most serious complications of long-term IBD (5). It has the third highest incidence of all malignant tumors (6). IBD is frequently diagnosed in 20-30-year-olds followed by another peak in 60-70-year-olds (7), where patients with IBD are at ~ three times higher risk of developing CRC compared with that in the general population (8,9).

Colonic inflammation is caused by an imbalance in the levels of proinflammatory and anti-inflammatory factors and is associated with the aberrant levels of interleukins (ILs) (10). Chronic inflammation of the mucosa is one of the main characteristics of IBD, the long-term presence of which can lead to carcinogenesis (11). CRC associated with colitis gradually develops from a negative test result for dysplasia,

to an indefinite test result for dysplasia, followed by the development of low-grade dysplasia, high-grade dysplasia and finally CRC (12). During the progression from inflammation to atypical hyperplasia and then CRC, the expression of NF-κB (13) and S11 calcium binding protein A9 (S100a9), which is a member of the S100 family known to serve roles in the innate immune system (14).

Traditional Chinese medicine and naturally-occurring compounds have been used to treat tumors because of their low risk of adverse effects and their therapeutic efficacy against multiple targets (15). *Evodia rutaecarpa* is a type of traditional Chinese medicine that has been used for the long-term treatment of gastrointestinal disorders, headaches and postpartum hemorrhage (16). In total, 131 compounds have been isolated and identified from the extract of *Evodia rutaecarpa*, with the majority consisting of alkaloids, terpenes and phenols (17). Evodiamine (Evo) is an alkaloid (Fig. 1A) that can be extracted from *Evodia rutaecarpa* (18). It can inhibit inflammation by inhibiting NF-κB (19), where it has been reported to exert anti-tumor activities against lung cancer, osteosarcoma, gastric cancer and breast cancer through the promotion of mitochondrial apoptosis (16). In addition, Evo has been demonstrated to inhibit inflammation by inhibiting the NLR family pyrin domain containing 3 inflammasome in mice with dextran sulfate sodium (DSS)-induced UC (19). However, the effects of Evo on CRC, including any possible underlying mechanisms, remain poorly understood.

In the present study, the potential effects of Evo in a mouse model of DSS-induced UC was examined. In addition, the possible effects of Evo on CRC were investigated in the C57BL/6-adenomatous polyposis coli (Apc)^{MinC}/Gpt strain of mice, which harbours a point-mutation in the *Apc* gene, which influences WNT-β-catenin signaling. Based on proteomics screening, the effects of Evo on inflammation, with emphasis on NF-κB signaling and S100a9 expression (which plays roles in the innate immune system), were studied. It is hoped that the data generated can provide experimental evidence for the potential clinical value of applying Evo for the treatment of UC or even CRC.

Materials and methods

Animal experiments

Establishment of the UC mouse model and agent administration procedure. In total, 75 male wild-type C57BL/6 mice (8 weeks old; mean weight ± standard error of mean, 23.1±0.3 g; weight range, 20-25 g) were supplied by Liaoning Changsheng Biotechnology Co., Ltd. [license no. SCXK (LIAO)-2015-0001; Liaoning, China]. The animals were housed in a specific pathogen-free (SPF) animal laboratory where they were allowed unrestricted access to food and water under a temperature of 22±2˚C and 40-60% humidity, with a 12-h light/dark cycle. Experimental protocols were approved by the Experimental Animal Ethics Committee of Jilin University (approval no. SY201905008).

Negative control mice received sterile water alone throughout the experimental period, whilst mice in the UC group were allowed to freely drink water containing 3% DSS (cat. no. S14048; Mw, 50,000 Da; Shanghai Yuanye Biological Technology Co., Ltd.) for 6 days. From the days 7 to 27, the mice with UC were fed water containing 3% DSS every 3 days and water without DSS the rest of the time. On day 7, mice with UC were randomly divided into four groups and were orally administered with either ddH_2O (model group; n=15), 0.6 g/kg sulfasalazine (SASP; cat. no. BP779; Mw, 398.39 Da; Sigma-Aldrich, Merck KGaA; positive control group, n=15), 10 mg/kg evodiamine (Evo; cat. no. B21315; Mw, 303.363 Da; Shanghai Yuanye Biological Technology Co., Ltd.; n=15) or 30 mg/kg Evo (n=15) once daily for the following 3 weeks. The dosage of Evo in this study was identified based on a previous study (19).

During the experimental period, body weight, fecal consistency and occult blood were evaluated daily. At the end of the experimental period, the mice were humanely euthanized and blood, colon, liver, spleen and kidney tissues were collected. The length of the colon was then measured. The euthanasia was performed according to the AVMA Guidelines for the Euthanasia of Animals (20), and the specific method was as follows: The mice were put into a CO_2-free euthanasia box, before the CO_2 was perfused at a rate of replacing 10-30% of the volume of the euthanasia box per min. After 5 min, if the mice were confirmed to be motionless, not breathing and with dilated pupils, the CO_2 would be turned off the mice would be observed for 2-3 min. The organ index values were calculated using the following formula: Organ index (%)=organ weight (g)/body weight (g) x100%.

The disease activity index (DAI) is a comprehensive score of weight loss, stool consistency and rectal bleeding that is used extensively to evaluate the clinical progress of patients with colitis (21,22). DAI values were calculated according to a previously described method (23). Scores were calculated as follows: Weight loss, 0 (no weight loss), 1 (1-5%), 2 (5-10%), 3 (10-15%), 4 (15-20%) and 5 (>20%); stool consistency, 0 (Normal stool), 1 (Mildly), 2 (Soft stool), 3 (Very soft stool), 4 (Watery stool) and 5 (Completely watery stool); rectal bleeding, 0 (Normal colored stool), 1 (Brown stool), 2 (Reddish stool), 3 (Mildly bloody stool), 4 (Bloody stool) and 5 (Very bloody stool). The DAI was calculated using the following formula: DAI=(weight loss + stool consistency + rectal bleeding)/3.

Establishment of the CRC mouse model and agent administration procedure. In total, 24 male C57BL/6-Apc^{MinC}/Gpt mice (8 weeks old; mean weight ± standard error of mean, 21.7±0.7 g; weight range, 20-25 g) were obtained from GemPharmatech Co., Ltd. [licence no. SCXK(SU)2018-0008; Nanjing, China]. Genetic testing and pathological sections were used to confirm the the successful establishment of the model. The animals were housed in a specific-pathogen-free animal laboratory (Jilin University, Changchun, China) and allowed unrestricted access to sufficient food and water under a temperature of 22±2˚C and 40-60% humidity, with a 12-h light/dark cycle. The experimental protocols were approved by the Experimental Animal Ethics Committee of Jilin University (approval no. SY201905003).

The C57BL/6-Apc^{MinC}/Gpt mice were randomly divided into two groups (n=12) and were orally administered with either ddH_2O (control group) or 10 mg/kg Evo every other day for 8 weeks. The body weight of the mice was recorded once a week. At the end of the experimental period, the mice were humanely euthanized, before blood, colon, liver, spleen and kidney tissues were collected. The organ index values were then calculated as aforementioned.

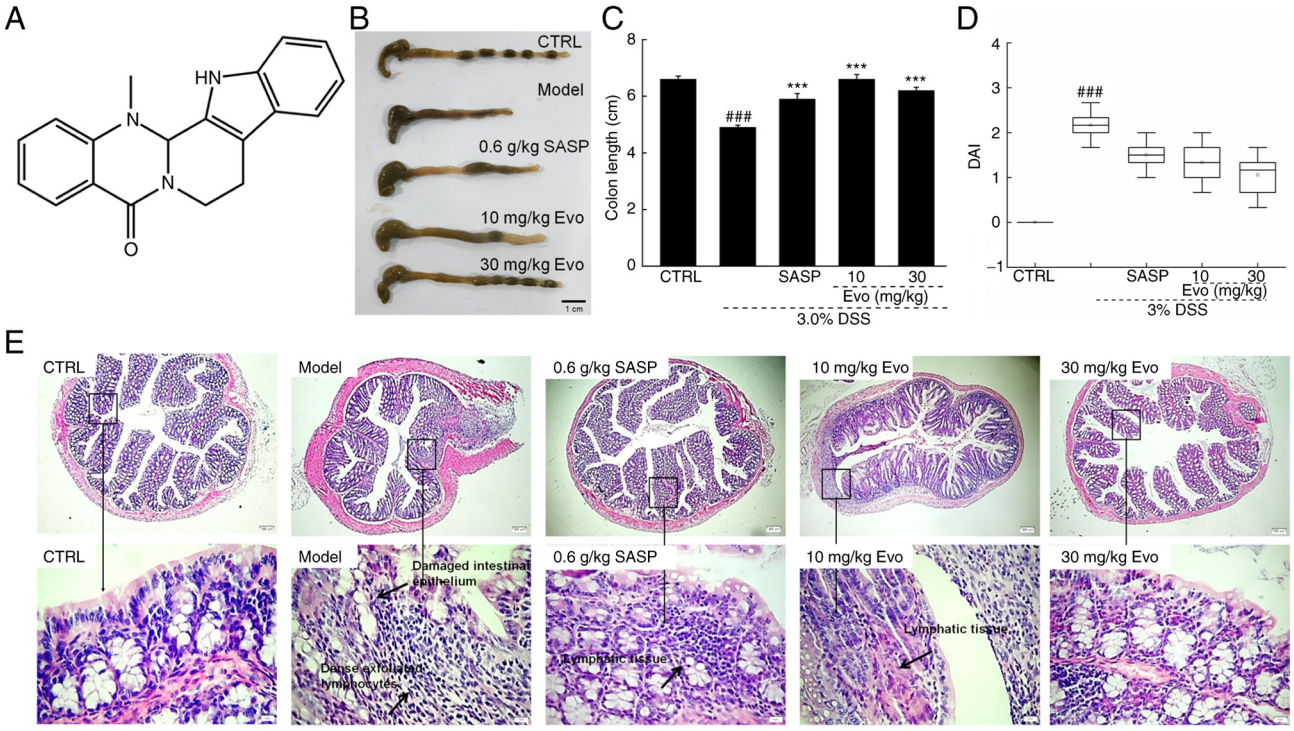

Figure 1. Protective effects of Evo against DSS-induced UC in mice. (A) The chemical structure of Evo. (B) Images of colons from mice in all five groups. (C) Evo reversed the reduction in colon length in mice with DSS-induced UC. Data are presented as the mean ± SEM (n=15) and were analyzed by a one-way ANOVA followed by Tukey's test. $^{###}$P<0.001 vs. CTRL; ***P<0.001 vs. 3.0% DSS-only. (D) Evo reversed the increase in DAI scores induced by DSS. Kruskal-Wallis test followed by Dunn's test was used to compare the differences in DAI among each group. $^{###}$P<0.001 vs. CTRL. (E) Evo alleviated pathological damage in the colonic epithelium of mice with UC. Histopathological observations of the colon (upper panel magnification, x40; lower panel magnifications, x400) tissues of mice with UC. Evo, evodiamine; DSS, dextran sodium sulfate; UC, ulcerative colitis; DAI, disease activity index; SASP, sulfasalazine.

Label-free quantification of proteins in the colons of UC mice. Colon tissue samples (n=3) from mice in the control, model and 10 mg/kg Evo-treated groups were fully lysed (25 mM Tris•HCl pH 7.6, 150 mM NaCl, 1% NP-40, 1% sodium deoxycholate, 1% SDS). Protein concentrations were determined using a BCA assay kit (cat. no. 23227; Thermo Fisher Scientific, Inc.) as previously described (24). A total of 100 μg total protein of each group was diluted to 1 mg/ml and mixed with 4 volumes of cold acetone. The mixture was thoroughly shaken at a low temperature (-20˚C; 30 min) and the proteins were precipitated by centrifugation at 4˚C at 10,000 x g for 10 min. The sediment was collected. The protein precipitate was re-dissolved in ammonium bicarbonate (100 mM ammonium bicarbonate, 1% sodium deoxycholate, pH 8.5), reduced (5 mM TCEP at 55˚C for 10 min), alkylated (10 mM iodoacetamide at room temperature for 15 min) and enzymatically hydrolyzed (2 μg trypsin solution at room temperature for 5 min; Promega Corporation). After removing sodium deoxycholate (the sodium deoxycholate was precipitated with 2% trifluoroacetic acid, centrifuged at 10,000 x g for 10 min at room temperature, and the supernatant was collected) from the peptide samples, they were desalted using a desalting column (cat. no. DC18150; Biocomma Limited) at room temperature.

The peptide samples prepared as aforementioned were analyzed using liquid chromatography-mass spectrometry (LC-MS)/MS (25). The details of the reaction were as follows: Nano-UPLC liquid phase system EASY-nLC1200 (Thermo Fisher Scientific, Inc.); positive ion detection mode; precursor scan range, 350-1,600 m/z; nitrogen gas temperature, 20˚C; spray voltage, 1.5 kv; flow rate, 300 nl/min. The results were processed using MaxQuant (1.5.6.0; Max Planck Institute of Biochemistry). The protein database is from the UNIPROT database (Uniprot_mouse_2016_09; https://www.uniprot.org/). The protein sequences and their inverted decoy sequences were used in the MaxQuant searches. Label-free quantification (LFQ) was used because it matches the samples between runs. The samples were normalized to keep the median total protein concentration in each group consistent before performing MaxQuant analysis and LFQ. Fold differences in protein concentrations were defined to be significant if the A/B ratio was >1.5 or <0.67. Subsequently, Gene Ontology (GO) (clusterProfiler_3.12.0; https://guangchuangyu.github.io/software/clusterProfiler/), Kyoto Encyclopedia of Genes and Genomes (KEGG) pathway (clusterProfiler_3.12.0; https://guangchuangyu.github.io/software/clusterProfiler/) and protein interaction analyses (STRINGdb_1.20.0; https://cn.string-db.org/cgi/input.pl) were performed. GO and KEGG used Fisher's precision probability test (P<0.05; n=3) and protein interaction analyses used random background model (no threshold filtering).

Detection of cytokines in serum and colon tissues of mice with UC and CRC. IL-1β (cat. no. KT2040-A), IL-2 (cat. no. KT2698-A), IL-6 (cat. no. KT2163-A), IL-8 (cat. no. KT2123-A), IL-15 (cat. no. KT2172-A), IL-17 (cat. no. KT2170-A), IL-22 (cat. no. KT9441-A), TNF-α (cat. no. KT2132-A), IFN-γ (cat. no. KT2182-A) concentrations in the colon tissues, which were

lysed using Radio Immunoprecipitation Assay (cat. no. R0010; Beijing Solarbio Science & Technology Co., Ltd.) containing 1% protease inhibitor cocktail (cat. no. P8340; Sigma-Aldrich; Merck KGaA) and 2% phenylmethanesulfonyl fluoride (cat. no. P7626; Sigma-Aldrich; Merck KGaA), and/or serum of mice with UC and CRC were measured using commercialized ELISA kits (Jiangsu Kete Bio-Technology Co., Ltd.) according to the manufacturer's protocols.

Histological analysis. Colon tissues were fixed with 4% paraformaldehyde for 48 h at room temperature and dehydrated using an ascending ethanol gradient from 50 to 100%. The tissues were cleared with xylene and embedded in paraffin wax blocks. Before staining, 5-μm thick colon tissue sections were dewaxed in xylene, rehydrated through a descending ethanol gradient from 100-70% and washed in PBS. This was followed by staining with hematoxylin for 6 min and eosin for 1 min at 20-25˚C in sequence and examined under a light microscope (magnification, x40 and x400; Olympus Corporation) as previously described (26).

Detection of apoptosis in colon tissues of mice with CRC. The extent of apoptosis in colon tissues of mice with CRC was detected using a Terminal Deoxynucleotidyl Transferase-Mediated dUTP *In Situ* Nick End Labelling Assay kit (cat. no. G1501; Wuhan Servicebio Technology Co., Ltd.) according to the manufacturer's protocols. Briefly, the sections prepared from colon tissues were retrieved with proteinase K for 22 min at 37˚C. Terminal deoxynucleotidyl transferase (TdT) enzyme and dUTP were added after breaking the membrane, and incubated at 37˚C for 2 h. Subsequently, the sections were washed with PBS three times for 5 min. The sections were then stained with DAPI (2 μg/ml) (cat. no. G1012; Wuhan Servicebio Technology Co., Ltd.) at room temperature and incubated without strong and direct light for 10 min. The sections were finally mounted with anti-fluorescence quenching mounting medium (cat. no. G1401; Wuhan Servicebio Technology Co., Ltd.). The fluorescent images were photographed using a fluorescence microscope (magnification, x200; Nikon Corporation).

Western blotting. Colon tissues of mice with UC and CRC were collected and washed immediately in D-Hank's buffer (8 g/l NaCl, 0.4 g/l KCl, 1 g/l glucose, 60 mg/l KH_2PO_4, 47.5 mg/l Na_2HPO_4, pH 7.2). The colon tissues were then lysed using Radio Immunoprecipitation Assay (cat. no. R0010; Beijing Solarbio Science & Technology Co., Ltd.) containing 1% protease inhibitor cocktail (cat. no. P8340; Sigma-Aldrich; Merck KGaA) and 2% phenylmethanesulfonyl fluoride (cat. no. P7626; Sigma-Aldrich; Merck KGaA), and protein concentration in the lysates was determined using a BCA protein assay kit, as previously described (24). The protein lysates (40 μg/lane) were resolved by 12% SDS-PAGE and transferred onto PVDF membranes. The membranes were blocked with 5% bovine serum albumin (cat. no. A8010; Beijing Solarbio Science & Technology Co., Ltd.) in Tris-buffered saline at 4˚C for 4 h and then incubated with primary antibodies against phosphorylated (p)-NF-κB (cat. no. ab86299; 1:4,000; Abcam), p-inhibitor NF-κB kinase α+β (IKKα+β; cat. no. ab195907; 1:500; Abcam), total (T)-NF-κB (cat. no. ab7970; 1:1,000), T-IKKα+β (cat. no. ab178870; 1:1,000; Abcam), p-IκBα (cat. no. ab12135; 1:500; Abcam), T-IκBα (cat. no. ab32518; 1:2,000; Abcam), GAPDH (cat. no. ab8245; 1:2,000; Abcam), S100a9 (cat. no. A9842; 1:1,000; ABclonal Biotech Co., Ltd.), Toll-like receptor 4 (TLR4; cat. no. bs-20594R, 1:2,000), myeloid differentiation factor 88 (MyD88; cat. no. bs-1047R, dilution: 1:300; BIOSS) overnight at 4˚C. They were then incubated with goat anti-rabbit IgG-HRP (cat. no. E-AB-1003; 1:5,000; Elabscience Biotechnology, Inc.) or goat anti-mouse IgG-HRP (cat. no. E-AB-1001; 1:5,000; Elabscience Biotechnology, Inc.) for 4 h at 4˚C. The bands were detected using an Ultrasensitive ECL Chemiluminescence Kit (cat. no. P10200; Suzhou New Saimei Biotechnology Co., Ltd.) and imaging system (BioSpectrum 600; BIOSS), and then quantified using Image J software (v1.8.0; National Institutes of Health).

Cell Culture. SW480 cells, a human colon adenocarcinoma cell line (The Cell Bank of Type Culture Collection of the Chinese Academy of Sciences), were cultured at 37˚C in a 5% CO_2 incubator with DMEM (cat. no. CM-0223B; Procell Life Science & Technology Co., Ltd.) containing 10% FBS (cat. no. 164210; Procell Life Science & Technology Co., Ltd.), 100 μg/ml streptomycin and 100 U/ml penicillin (Thermo Fisher Scientific, Inc.).

Cell viability assay. SW480 cells were seeded into 96-well plates at the density of $8x10^3$ cells/well and treated with Evo at doses of 20-200 μM for 24 h at 37˚C. Cell viability was detected using MTT assay (26). Briefly, MTT was added (5 mg/ml) to 96-well plates and incubated for 4 h at 37˚C. Subsequently, the liquid was aspirated, dissolved in DMSO and the optical density value at 490 nm was measured.

Mitochondrial membrane potential (MMP) detection. SW480 cells were seeded into six-well plates at a density of $2x10^5$ cells/well and treated with 100 and 200 μM Evo for 12 h at 37˚C. The collected cells were incubated with the JC-1 dye (Final concentration, 5 μg/ml; cat. no. BB-4105; BestBio) at 37˚C for 20 min in the dark and then washed with PBS for three times. A fluorescence microscope (magnification, x100; Nikon Corporation) was used to observe the fluorescence intensity of the cells (brighter red fluorophores represent higher mitochondrial membrane potential).

Cell cycle detection. SW480 cells were seeded into six-well plates at a density of $2x10^5$ cells/well and treated with 100 and 200 μM Evo for 12 h at 37˚C. Collected cells were washed with ice-cold PBS and incubated with 70% pre-cooled ethanol for >3 h at -20˚C. The cells were then exposed to the Muse® Cell Cycle Reagent (cat. no. MCH100106; MilliporeSigma) at room temperature for 30 min in the dark. Muse® Cell Analyzer (cat. no. 0500-3115; MilliporeSigma) was used to detect the conditions of the cell cycle.

Immunofluorescence of p-NF-κB. Immunofluorescence of p-NF-κB was performed using a NF-κB Activation, Nuclear Translocation Assay Kit (cat. no. SN368; Beyotime Institute of Biotechnology). Briefly, SW480 cells were seeded into glass-bottom cell culture dishes at a seeding density of $2x10^5$ cells/well and treated with 100 and 200 μM Evo for

12 h at 37˚C. Collected cells were washed with ice-cold PBS and then incubated with the primary NF-κB p65 antibody (undiluted) at 4˚C overnight after fixing (cold 100% methanol at -20˚C) for 10 min and blocking (5% BSA) for 60 min at 37˚C. The cells were then incubation with a Cy3-conjugated secondary antibody (undiluted) for 1 h at room temperature. Subsequently, the cells were stained with DAPI (undiluted) for 5 min at room temperature and then visualized by a confocal microscope (magnification, x400; LSM710; Carl Zeiss AG).

Statistical analysis. All data are presented as the mean ± standard error of the mean (SEM). *In vitro*, all experiments were repeated six times. Kruskal-Wallis test followed by Dunn's test was used to compare differences in the DAI among each group. One-way analysis of variance and Tukey's post hoc multiple comparisons test were performed using the SPSS 16.0 software (SPSS, Inc.) in other data. $P<0.05$ was considered to indicate a statistically significant difference.

Theoretical analysis. The three-dimensional structure of NF-κB (NCBI no. NP_033071.1) was built using the online tool SWISS-MODEL (release date, 2017-03-08; https://swissmodel.expasy.org/). The template and the structure of the complex between the kinase-inducible domain-interacting domain of CREB binding protein (CBP) (PDB ID, 5U4K) and the transactivation domain 1 of p65 showed 93.33% sequence identify (27). The ligand, Evo, which was downloaded from chemspider (http://www.chemspider.com/), was docked onto T-NF-κB and p-NF-κB (S536P) using AutoDock 4.2 (Olson Lab at the Scripps Institute; https://autodock.scripps.edu/) (28,29). The size of the docking box was set to 20x20x25 and the length of each grid was 0. 0375 nm. The molecular docking was calculated by the Lamarckian genetic algorithm. Amber 16 software (Amber is developed in an active collaboration of David Case at Rutgers University; http://ambermd.org/) was used to analyze the four systems, T-NF-κB, p-NF-κB, T-NF-κB-Evo and p-NF-κB-Evo (30) for 50 nsec molecular dynamics (MD) simulations. The amber ff99SB forcefield, which could give a force to an atom before MD, was applied to the proteins and ligands (31).

Results

Effects of Evo on DSS-induced UC. DAI and weight loss are important parameters used to evaluate the degree of inflammation in patients with UC (32,33). Compared with that in healthy mice, significant weight loss (Table SI), significant reductions in colon length (Fig. 1B and C) and increased DAI scores on day 27 (Fig. 1D) were observed in mice with DSS-induced UC. These symptoms were ameliorated after Evo administration (Fig. 1B-D and Table SI).

Furthermore, mice with DSS-induced UC showed a damaged intestinal epithelium, fewer numbers of goblet cells and dense exfoliated lymphocyte infiltration into the submucosa (Fig. 1E). By contrast, both SASP and Evo treatment markedly improved these pathologic changes in the colon tissues (Fig. 1E).

Anti-UC effects of Evo is associated with NF-κB signaling. In the colon tissue samples analyzed, 23,519 peptides, 3,375 groups of proteins, 3,316 quantifiable proteins and 838 differentially expressed proteins were identified. The administration of Evo at a dose of 10 mg/kg significantly increased the levels of 129 proteins and decreased the levels of 129 proteins in the colons of mice with DSS-induced UC (Fig. 2A and Table SII). Through STRINGdb analysis of protein interactions between the groups, potent interactions were found among 258 molecules in the colons between the UC model and Evo-treated UC mice (Figs. 2B and S1). GO enrichment analysis showed that the 258 proteins with significantly changed expression levels were associated with 'response to IFN-β', 'cellular response to IFN-β', 'mitochondrial inner membrane' and 'organelle inner membrane' (Fig. 3A). According to KEGG enrichment analysis, Evo altered processes in 'oxidative phosphorylation', 'human papillomavirus infection' and 'lysosome' (Fig. 3B). These results suggest that Evo may reduce the inflammatory response in UC.

Compared with healthy mice, significantly increased levels of IL-1β, IL-2, IL-6, IL-8 and TNF-α were observed in the colon tissues of mice with UC (Fig. 4A-F). However, 3 weeks of Evo administration resulted in significant reductions in the colonic levels of IL-1β, IL-2, IL-6, IL-8, TNF-α and IFN-γ (Fig. 4A-F). However, *ad libitum* drinking of DSS only caused a significant increase in the concentration of IL-1β in the serum (Table SIII). In addition, Evo treatment significantly reduced the serum concentrations of IL-1β, IL-6 and IL-8 in mice with DSS-induced UC (Table SIII).

NF-κB is considered to be a key regulator of inflammation (11). Evo significantly reduced the phosphorylation of NF-κB, IKKα/β and IκBα and the expression levels of S100a9, TLR4 and MyD88 in the colon tissues of mice with UC compared with those in vehicle-treated mice with UC (Fig. 4G).

Anti-CRC effects of Evo in Apc^{MinC}/Gpt mice through NF-κB signaling. Evo significantly reduced the viability of SW480 cells (Fig. S2A) and caused cell cycle arrest at the G_2/M phase (Fig. S2B). In addition, Evo inhibited mitochondrial membrane potential (Fig. S2C), reduced the expression of p-NF-κB and suppressed the translocation of p-NF-κB from the cytoplasm to the nucleus (Fig. S2D) in SW480 cells.

Apc^{MinC}/Gpt mice, which spontaneously develop colorectal tumors, were used in the present study to examine the effects of Evo on CRC (34). After 8 weeks of Evo administration, the numbers and sizes of the colonic tumors were markedly reduced (Fig. 5A and F), whereas the degree of weight loss in the Apc^{MinC}/Gpt mice was significantly lower (Fig. 5B). Evo also significantly reduced the liver (Fig. 5C) and kidney index values (Fig. 5D). In addition, Evo significantly enhanced the spleen index values (Fig. 5E) of mice with CRC, suggesting that the administration of Evo reduced inflammation. Compared with that in the control mice, an increase in green fluorescence representing apoptotic cells in tumor tissues was observed, indicating that Evo administration promoted tumor tissue apoptosis (Fig. S3).

Compared with vehicle-treated Apc^{MinC}/Gpt mice with CRC, 8 weeks of Evo administration significantly suppressed the serum concentrations of IL-1β, IL-6, IL-22 and TNF-α whilst significantly increasing the concentration of IL-15 (Fig. 6A-G). In colonic tissues, Evo administration significantly reduced the levels of IL-1β, IL-2, IL-6, IL-17, IL-22

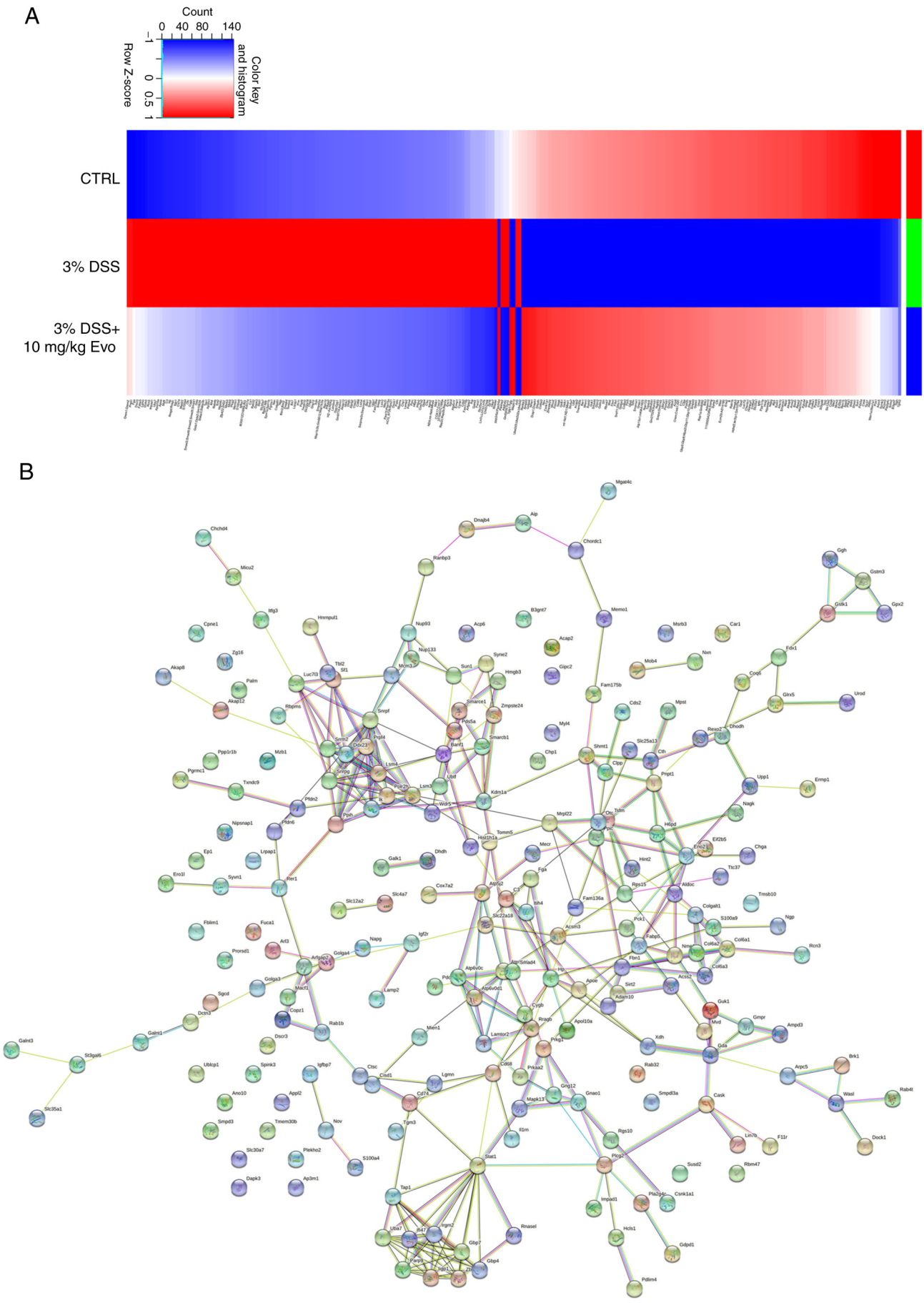

Figure 2. Proteomic analysis of the factors significantly regulated by Evo in mice with ulcerative colitis. (A) Heatmap of proteins markedly different between control, model and Evo-treated group (n=3). Red represents promotion and blue represents inhibition. (B) The relationship between the proteins were processed through STRINGdb (the simplified network) (n=3). Evo, evodiamine; DSS, dextran sodium sulfate; CTRL, control.

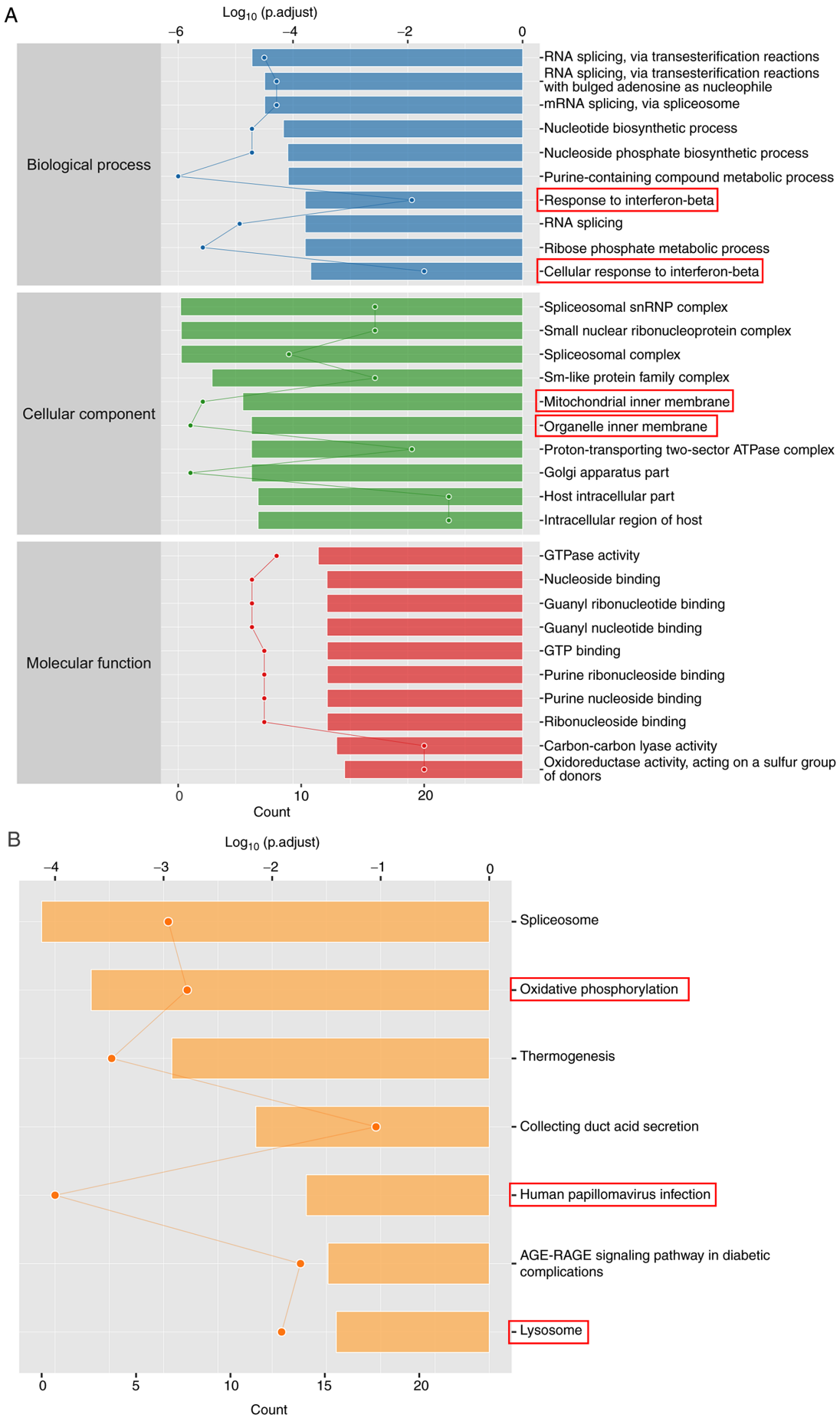

Figure 3. Enrichment analysis of the factors significantly regulated by Evo in mice with ulcerative colitis. (A) GO enrichment and (B) KEGG analyses (n=3) of mice with ulcerative colitis in colon tissues. GO, Gene Ontology; KEGG, Kyoto Encyclopedia of Genes and Genomes.

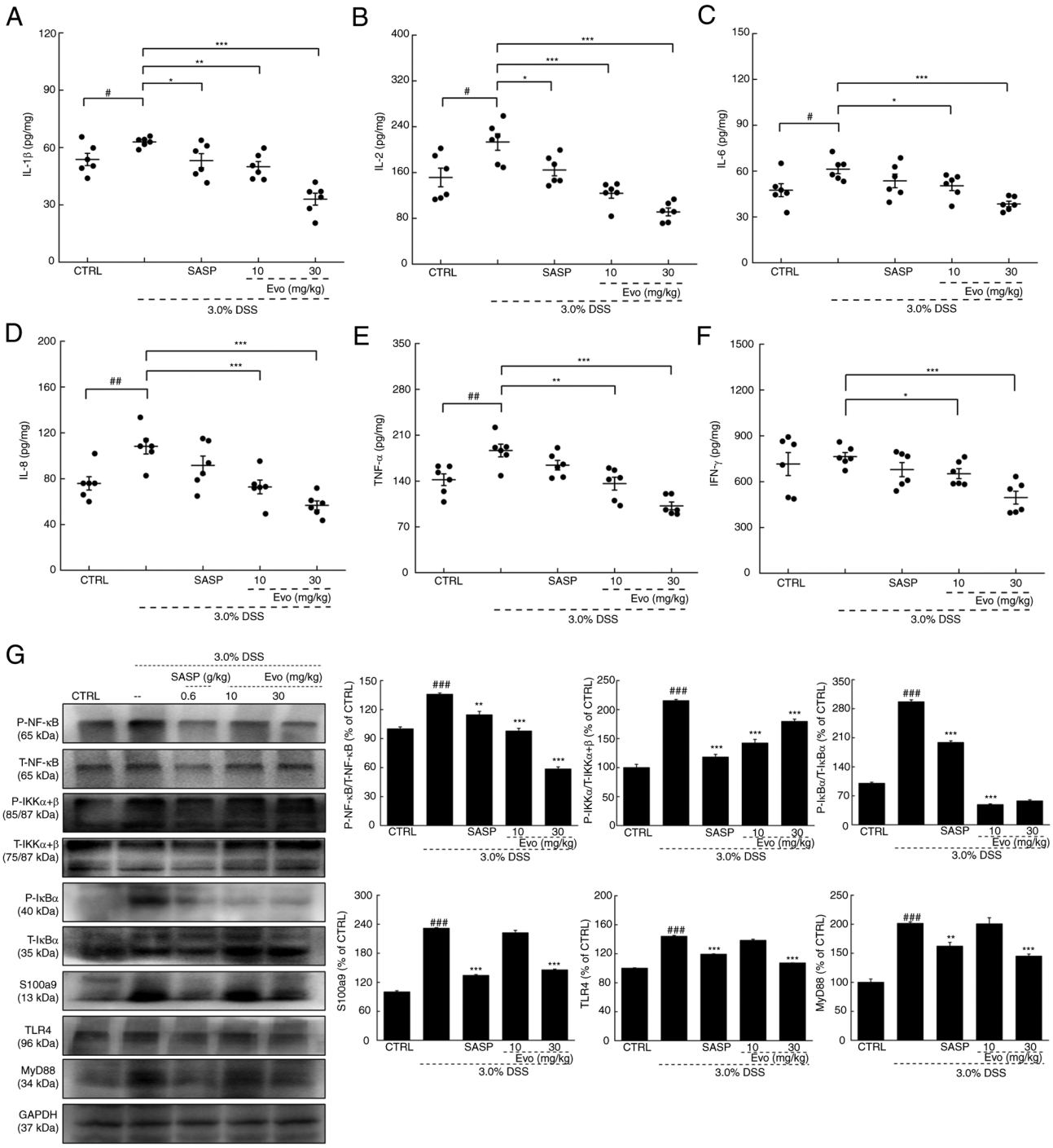

Figure 4. Evo ameliorates inflammation in the colonic tissues of mice in UC. Evo reduced the levels of (A) IL-1β, (B) IL-2, (C) IL-6, (D) IL-8, (E) TNF-α and (F) IFN-γ in the colonic tissues of mice with UC (n=6). (G) Evo exerted anti-inflammatory effects by inhibiting NF-κB signaling. Compared with their levels in vehicle-treated mice with UC, Evo reduced the phosphorylation levels of NF-κB, IKKα/β and IκBα and the expression levels of S100a9, TLR4 and MyD88 in the colons of mice with UC (n=3). The levels of each protein were normalized to those of GAPDH. Data are presented as the mean ± SEM and were analyzed using one-way ANOVA followed by Tukey's test. $^{\#}$P<0.05, $^{\#\#}$P<0.01 and $^{\#\#\#}$P<0.001 vs. CTRL; *P<0.05, **P<0.01 and ***P<0.001 vs. 3.0% DSS-only. Evo, evodiamine; DSS, dextran sodium sulfate; CTRL, control; UC, ulcerative colitis; SASP, sulfasalazine; p-, phosphorylated; t-, total; TLR4, Toll-like receptor 4; MyD88, myeloid differentiation primary response 8; S100a9, S100 calcium binding protein A9; IκBα, inhibitor of NF-κBα; IKK, IκB kinase.

and TNF-α, but significantly increased the expression levels of IL-15 (Fig. 6A-G).

The NF-κB pathway has been reported to regulate the expression of oncogenes and proinflammatory genes (11). IL-6-activated NF-κB has been previously found to promote the development of CRC by acting on intestinal epithelial cells (35). During the development of CRC, constitutive activation of this pathway promotes the malignant transformation and proliferation of colonic epithelial cells (36). Following 8 weeks of Evo administration, the phosphorylation levels of NF-κB, IKKα/β and IκBα were significantly reduced and the expression levels of S100a9 were also significantly reduced, in the colon compared with those in vehicle-treated Apc^{MinC}/Gpt mice with CRC (Fig. 6H).

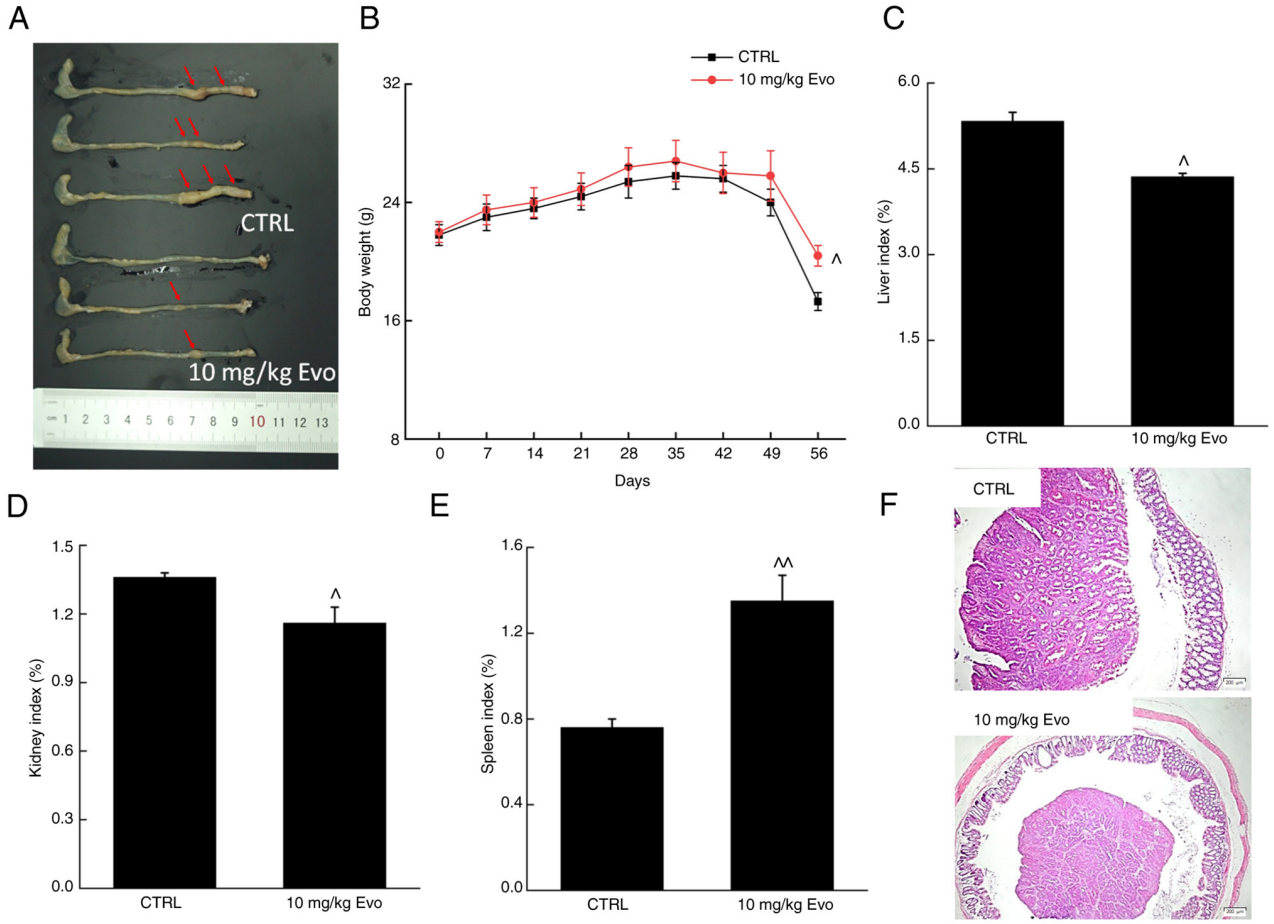

Figure 5. Anti-tumor effect of Evo against CRC in Apc^{MinC}/Gpt mice. (A) Evo reduced the number of tumors and the sizes of the colon, (B) suppressed weight loss, decreased the (C) liver and (D) kidney index values, whilst increasing the (E) spleen index values in Apc^{MinC}/Gpt mice with CRC. (F) Histopathological observation of the colon tissues of Apc^{MinC}/Gpt mice after treatment with Evo (magnification, x40). Data are presented as the mean ± SEM (n=6) and were analyzed using one-way ANOVA followed by Tukey's tests. $^{\wedge}$P<0.05 and $^{\wedge\wedge}$P<0.01 vs. CTRL mice. CRC, colorectal cancer; Evo, evodiamine; CTRL, control.

MD simulations. Theoretical models were built to explain the inhibition of NF-κB activation by Evo. Sequence alignment between the templates, XP_004627287.1 and XP_020020483.1 (the closest protein number which compared in Blast) and NF-κB is shown in Fig. 7A, whereas the docking of Evo onto NF-κB is shown in Fig. 7B. Asp533, Ile537, Phe534 and Ser536 (phosphorylated residue) were found to be important residues for Evo binding. The effects of the protein chains and the solvent environment on the secondary structure of the protein were subsequently determined (Fig. 7C and D). Evo binding to either T-NF-κB or p-NF-κB may increase the probability of α helix formation. To confirm whether the conformational changes were continuous and stable, principal components analysis and cross-correlation analyses were further performed. The cross-correlation analyses of the four systems indicated that the significant movement mainly occurred between the regions of the α helix (Fig. 7E). According to free energy landscape model, the structures of the two most stable conformations of Evo binding to T-NF-κB and p-NF-κB revealed that the conformational changes in the α helix existed during MD simulations (Fig. 7F).

Discussion

The present study systemically investigated effects of Evo on inflammation, UC and CRC, with focus on NF-κB signaling. Inflammation has been reported to regulate every stage of tumor development, from initiation to and metastasis (37). A number of pathways, including NF-κB, are activated during chronic inflammation, which can promote tumor development by promoting epithelial cell proliferation and angiogenesis (11). During the early events of the development of colitis-associated CRC, the *TP53* gene is mutated, leading to the constitutive activation of NF-κB and increased inflammation (35). This inflammatory environment can potentiate DNA damage and ultimately lead to mutations in the *APC* gene and tumor initiation (35). *APC* is a frequently mutated gene in human sporadic CRC and is almost always mutated in familial *APC* (38). The loss of *APC* function is frequently an early event in the pathogenesis of CRC.

Epithelial cells and immune cells in the intestines of mice with colitis express a variety of proinflammatory mediators (39). As an effective NF-κB activator, IL-1β appears during the early stages of intestinal inflammation and sustains the inflammatory environment in colonic tissues (40). High expression levels of IL-1β have been observed in the tumors from mice with DSS/azoxymethane-induced colitis-associated CRC and in non-colitic APC$^{\Delta 468}$ mice (41). IL-1β promotes the production of IL-6 (41), which contributes to the development of IBD and the tumorigenesis of CRC through its receptor, IL-6R (42). Both IL-1β and IL-6 levels were found to be

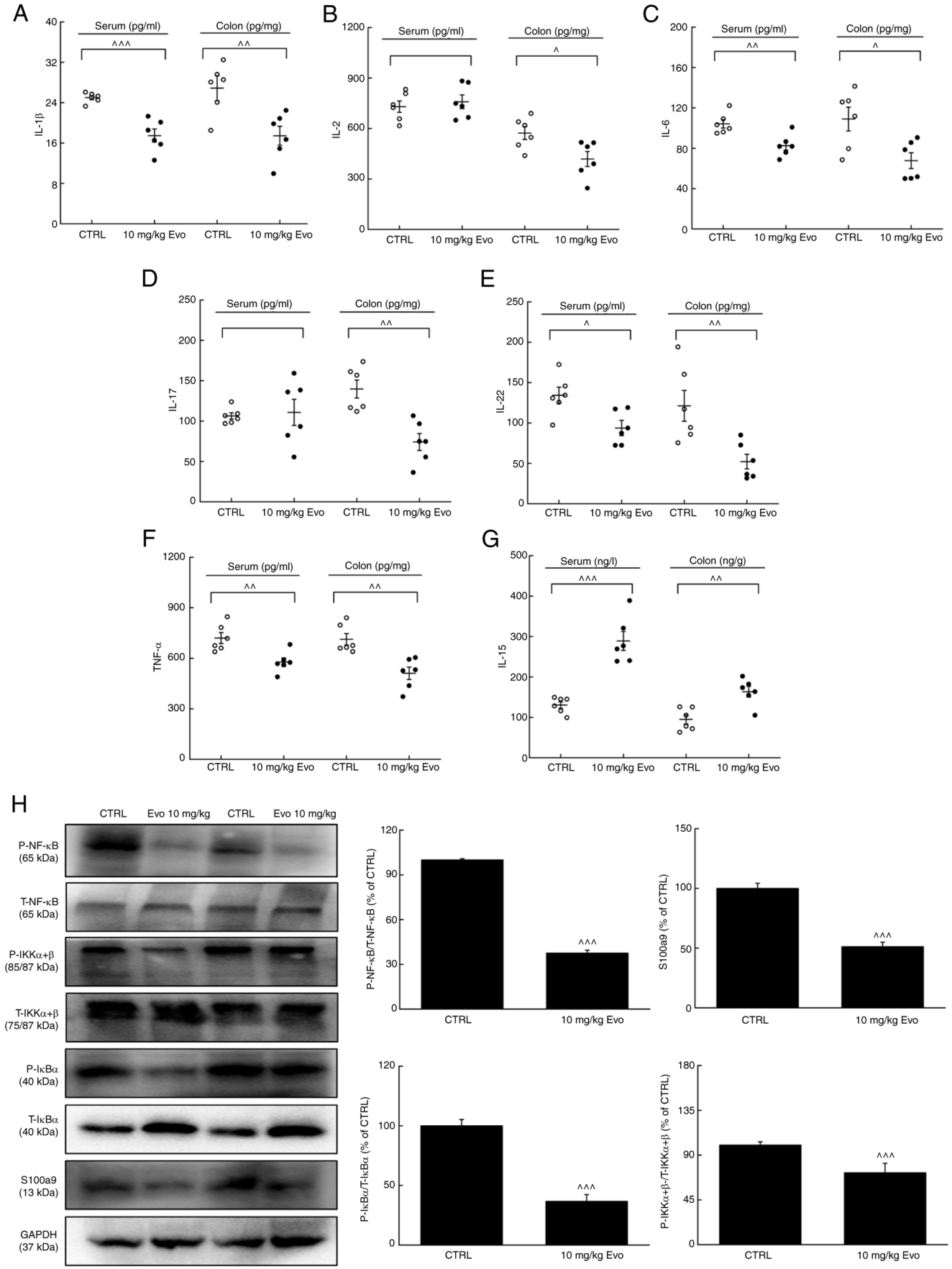

Figure 6. Evo exerts anti-inflammatory effects in Apc^{MinC}/Gpt mice by inhibiting NF-κB signaling. Evo reduced the levels of (A) IL-1β, (B) IL-2, (C) IL-6, (D) IL-17, (E) IL-22 and (F) TNF-α, whilst increasing the levels of (G) IL-15 in the serum and colon samples of Apc^{MinC}/Gpt mice (n=6). (H) Evo suppressed the phosphorylation of NF-κB, IKKα/β and IκBα and the expression levels of S100a9 in colonic tissues (n=3). Data are presented as the mean ± SEM and were analyzed by one-way ANOVA followed by Tukey's test. $^{\wedge}P<0.05$, $^{\wedge\wedge}P<0.01$ and $^{\wedge\wedge\wedge}P<0.001$ vs. CTRL. Evo, evodiamine; CTRL, control; S100a9, S100 calcium binding protein A9; p-, phosphorylated; t-, total; IκBα, inhibitor of NF-κBα; IKK, IκB kinase.

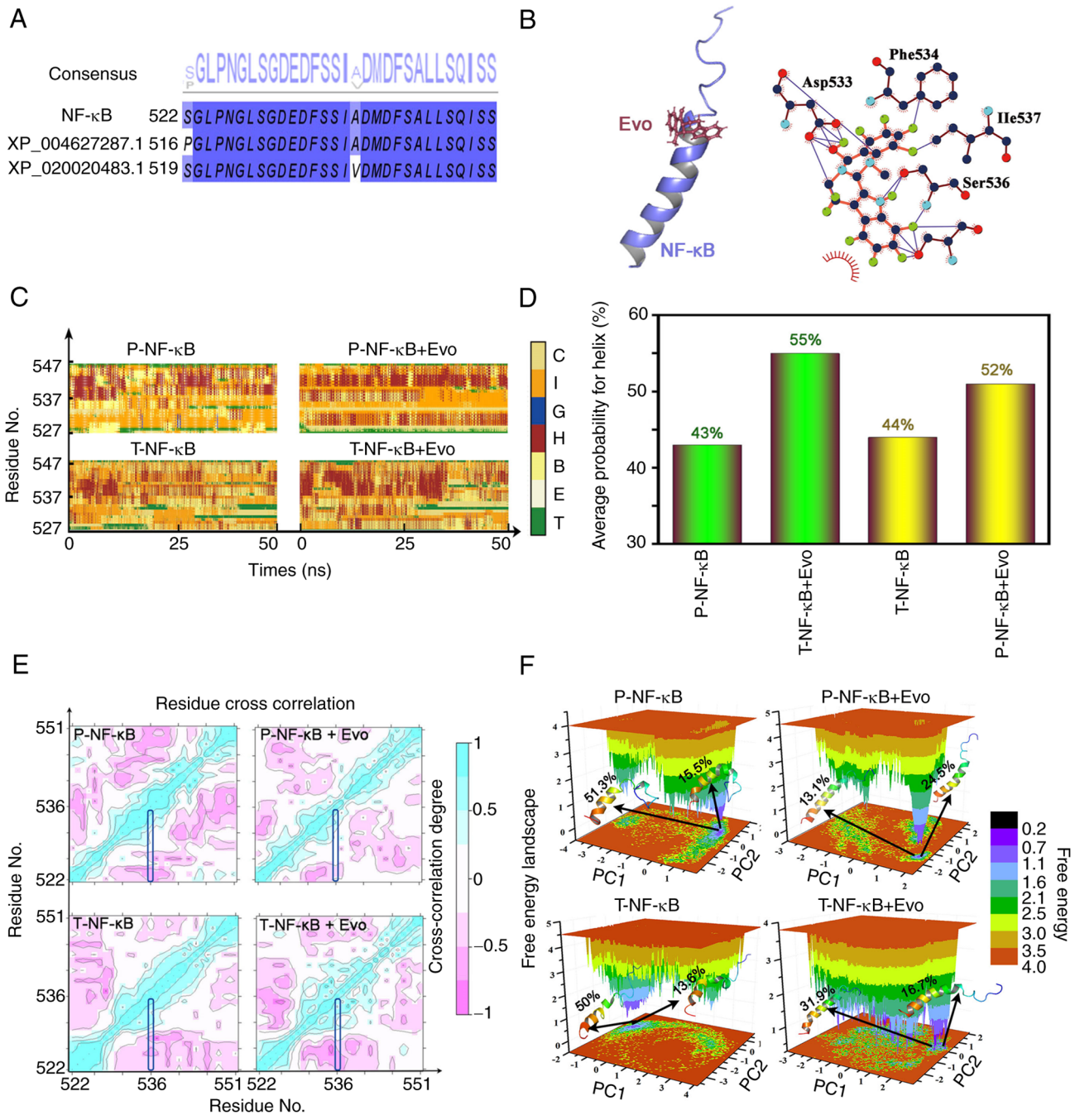

Figure 7. Docking data of Evo onto NF-κB. (A) Sequence alignment of NF-κB, XP_004627287.1 and XP_020020483.1 (the closest protein number which compared in Blast). (B) The structure of the complex and the potential interaction between NF-κB and Evo. (C) Changes in the secondary structure of T-NF-κB, T-NF-κB + Evo, p-NF-κB and p-NF-κB + Evo. (D) The average probability of a helix which might influence the NF-κB in T-NF-κB, T-NF-κB + Evo, p-NF-κB, and p-NF-κB + Evo. (E) Cross-correlation maps for T-NF-κB, T-NF-κB + Evo, p-NF-κB, and p-NF-κB + Evo. (F) Free energy landscape for T-NF-κB, T-NF-κB + Evo, p-NF-κB, and p-NF-κB +Evo. Evo, evodiamine; T-total; p-, phosphorylated; C, coil; I, 5-helix; G, 3-helix; H, α-helix; B, β-bridge; E, β-sheet; T, turn.

suppressed by Evo administration in mice with UC and CRC in the present study.

TNF-α is an effective proinflammatory cytokine that serves important roles in immune regulation, the inflammatory response, proliferation and death of all cell types (43). The levels of TNF-α are frequently found to be elevated in the blood, stool samples and mucous membranes of patients with UC (44). The production and release of TNF-α is stimulated by IFN-γ and IL-1 (43), where TNF-α activates NF-κB through TNF receptor-related factor 2 (45). TNF-α is also an effective activator of intestinal epithelial cells where it stimulates the production of the proinflammatory cytokine IL-8, which is a key mediator of inflammation in the C-X-C chemokine family (46). An association between the severity of inflammation and the levels of IL-8 in the colonic mucosa has been reported, where elevated IL-8 levels have been found in the colonic mucosa of patients with UC (47). However, upon stimulation, the production of a large amounts of IL-8 is induced, which chemotactically attracts polymorphonuclear leukocytes, monocytes and macrophages to the site of inflammation, where

IL-8 then aggravates the inflammation (48). The promoter region of IL-8 has binding sites for transcription factors, such as activator protein 1 and NF-κB (48). Once activated, NF-κB may cause the overexpression of proinflammatory cytokines, thereby promoting a Th1-dependent lymphocyte immune response (49). IL-6 promotes the chemotaxis of neutrophils, promotes colonic necrosis and ultimately tissue destruction (50). In the present study, the inhibitory activity of Evo on NF-κB was noted in the DSS-induced mouse UC model. Evo improved the symptoms of UC by inhibiting the DSS-induced activation of NF-κB, downregulating the levels of proinflammatory genes IL-1β, IL-6, IL-8 and TNF-α whilst preventing the infiltration of inflammatory cells.

In Apc^{MinC}/Gpt mice with CRC, Evo further promoted the levels of IL-15 and inhibited IL-17 and -22 in the serum and colonic tissues according to the results of ELISA. IL-15 enhances the proliferation and activation of natural killer cells and CD8+ T cells, which in turn promote humoral and cell-mediated immune responses, thereby inhibiting tumor growth (41). The loss of or reduction in IL-15 expression in human CRC results in higher risks of recurrence (41). In sporadic CRC, mutations in the *APC* gene cause the loss of cell polarity and tight junctions, leading to bacterial invasion and production of IL-17 (35). In IBD, high levels of IL-17 have been found in the inflamed intestinal mucosa (51). Accordingly, the simultaneous neutralization of IL-17 and TNF-α may switch off NF-κB signaling, which may negate the mitogenic effects of factors secreted by CRC cells (52). Furthermore, Evo strongly suppressed the levels of IL-22, which is found at high levels in the serum and intestines of patients with IBD (52). IL-22 expression has also been found to be upregulated in leukocytes infiltrating the tumor mass in patients with colitis-related CRC (11). The activation of IL-22R in turn leads to an increase in IL-8 and TNF-α levels (51). These results suggest that the suppression of NF-κB signaling serves an important role in mediating the anti-CRC effects of Evo in Apc^{MinC}/Gpt mice.

Furthermore, the dysregulation of S100a9, a Ca^{2+}-binding protein of the S100 family that controls acute and chronic inflammation, has been widely observed in IBD (3). S100a8/a9 functions as an 'alarm' protein at the site of the inflammation by activating TLR4 (53), which subsequently activates NF-κB (54). In colonic tissues of mice with UC or CRC, Evo markedly regulated the levels of S100a9, p-NF-κB and its upstream proteins. TLR4, a lipopolysaccharide receptor, is expressed at high levels in the colonic tissues of patients with UC and mice with DSS-induced colitis (55). The activation of TLR4 promotes the signaling cascade mediated by MyD88, which leads to the activation of NF-κB and the release of IL-6 (56). NF-κB expression and activation are markedly increased in the inflamed intestines of patients with IBD, in addition to those animals of experimental colitis models (11). Once NF-κB is activated, the NF-κB inhibitor, IκB, which binds to NF-κB, is also phosphorylated by the IKK complex. p-IκB causes the translocation of NF-κB to the nucleus, where it activates the transcription of related target genes encoding inflammatory factors, especially IL-6 (57). In SW480 cells, Evo exposure potently suppressed the translocation of p-NF-κB from the cytoplasm into the nucleus. Experimental and theoretical data in the present study suggest that Evo may directly inhibit the phosphorylation of NF-κB. It has been reported that phosphorylated serine can promote electron transfer, since they facilitate the formation or destruction of various non-bonding interactions (58). Evo binding to p-NF-κB may induce new interactions with NF-κB, which facilitate the formation of an α helix in p-NF-κB, as indicated by MD simulations.

There are a number of limitations in the present study. It only investigated the effects of Evo on UC and CRC in relation to NF-κB signaling from the perspective of inflammation. However, because of the selection of animal models, an in-depth study of the role of Evo in the transition from UC to colitis-related CRC was not possible. In addition, the effects of mitochondrial function on the anti-inflammatory effects of Evo would require further study.

Altogether, data from the present study suggest that Evo can reduce the inflammatory response in UC and CRC by preventing damage of the intestinal mucosal barrier and by regulating the secretion of inflammatory cytokines. The suppression on the activation of NF-κB serve central roles in mediating these effects. The findings provide experimental evidence that Evo may be promising as an effective treatment option in clinics for colitis and CRC.

Acknowledgements

Not applicable.

Funding

The present study was supported by the Science and Technology Development Project of Jilin Province in China (grant nos. 20200708037YY, 20200708068YY and 20200708091YY) and the Natural Sciences Foundation of Jilin Province in China (grant nos. 20200201030JC and 20200201122JC).

Availability of data and materials

The datasets used and/or analyzed during the current study are available from the corresponding author on reasonable request. The datasets generated and/or analyzed during the current study are available in the ProteomeXchange Consortium via the PRIDE partner repository (dataset identifier PXD027745), (Username, reviewer_pxd027745@ebi.ac.uk; Password, pZmVuoRu; https://www.ebi.ac.uk/pride/archive).

Authors' contributions

CL and YQ contributed to the conceptual design of the research. YonZ, YaqZ, YanZ, WW, WM and YuZ performed the experiments. YonZ and YaqZ processed the data. YonZ and YaqZ wrote the manuscript. WM and YuZ helped perform the analysis with constructive discussions. YonZ and YaqZ confirm the authenticity of all the raw data. All authors read and approved the final version of the manuscript.

Ethics approval and consent to participate

All the animal experiments have been approved by the Experimental Animal Ethics Committee of Jilin University (approval nos. SY201905008 and SY201905003).

Patient consent for publication

Not applicable.

Competing interests

The authors declare that they have no competing interests.

References

1. Yue B, Ren YJ, Zhang JJ, Luo XP, Yu ZL, Ren GY, Sun AN, Deng C, Wang ZT and Dou W: Anti-inflammatory effects of fargesin on chemically induced inflammatory bowel disease in mice. Molecules 23: 1380, 2018.
2. Xavier RJ and Podolsky DK: Unravelling the pathogenesis of inflammatory bowel disease. Nature 448: 427-434, 2007.
3. Zhang X, Wei L, Wang J, Qin Z, Wang J, Lu Y, Zheng X, Peng Q, Ye Q, Ai F, *et al*: Suppression colitis and colitis-associated colon cancer by anti-S100a9 antibody in mice. Front Immunol 8: 1774, 2017.
4. Bernstein CN, Fried M, Krabshuis JH, Cohen H, Eliakim R, Fedail S, Gearry R, Goh KL, Hamid S, Khan AG, *et al*: World gastroenterology organization practice guidelines for the diagnosis and management of IBD in 2010. Inflamm Bowel Dis 16: 112-124, 2010.
5. Zhao Y, Guo Q, Zhao K, Zhou Y, Li W, Pan C, Qiang L, Li Z and Lu N: Small molecule GL-V9 protects against colitis-associated colorectal cancer by limiting NLRP3 inflammasome through autophagy. Oncoimmunology 7: e1375640, 2017.
6. Doubeni CA, Laiyemo AO, Major JM, Schootman M, Lian M, Park Y, Graubard BI, Hollenbeck AR and Sinha R: Socioeconomic status and the risk of colorectal cancer: An analysis of more than a half million adults in the national institutes of health-AARP diet and health study. Cancer 18: 3636-3644, 2012.
7. Assadsangabi A and Lobo AJ: Diagnosing and managing inflammatory bowel disease. Practitioner 257: 13-18, 2, 2013.
8. Porta C, Ippolito A, Consonni FM, Carraro L, Celesti G, Correale C, Grizzi F, Pasqualini F, Tartari S, Rinaldi M, *et al*: Protumor steering of cancer inflammation by p50 NF-κB enhances colorectal cancer progression. Cancer Immunol Res 6: 578-593, 2018.
9. Vilarrasa Rull E and González Lama Y: Clinical features of hidradenitis suppurativa and Crohn disease: What do these two entities have in common? Actas Dermosifiliogr 107 (Suppl 2): S21-S26, 2016 (In English, Spanish).
10. Pichai MV and Ferguson LR: Potential prospects of nanomedicine for targeted therapeutics in inflammatory bowel diseases. World J Gastroenterol 18: 2895-2901, 2012.
11. Luo CX and Zhang H: The role of proinflammatory pathways in the pathogenesis of colitis-associated colorectal cancer. Mediators Inflamm 2017: 5126048, 2017.
12. Bressenot A, Cahn V, Danese S and Peyrin-Biroulet L: Microscopic features of colorectal neoplasia in inflammatory bowel diseases. World J Gastroenterol 20: 3164-3172, 2014.
13. Cho HT, Kim JH, Heo W, Lee HS, Lee JJ, Park TS, Lee JH and Kim YJ: Explosively puffed ginseng ameliorates ionizing radiation-induced injury of colon by decreasing oxidative stress-related apoptotic cell execution in mice. J Med Food 22: 490-498, 2019.
14. Duan L, Wu R, Ye L, Wang H, Yang X, Zhang Y, Chen X, Zuo G, Zhang Y, Weng Y, *et al*: S100A8 and S100A9 are associated with colorectal carcinoma progression and contribute to colorectal carcinoma cell survival and migration via Wnt/β-catenin pathway. PLoS One 8: e62092, 2013.
15. Lu Y, Li CS and Dong Q: Chinese herb related molecules of cancer-cell-apoptosis: A minireview of progress between Kanglaite injection and related genes. J Exp Clin Cancer Res 27: 31, 2008.
16. Jiang J and Hu C: Evodiamine: A novel anti-cancer alkaloid from *Evodia rutaecarpa*. Molecules 14: 1852-1859, 2009.
17. Zhao Z, He X, Han W, Chen X, Liu P, Zhao X, Wang X, Zhang L, Wu S and Zheng X: Genus tetradium L.: A comprehensive review on traditional uses, phytochemistry, and pharmacological activities. J Ethnopharmacol 231: 337-354, 2019.
18. Yu H, Jin H, Gong W, Wang Z and Liang H: Pharmacological actions of multi-target-directed evodiamine. Molecules 18: 1826-1843, 2013.
19. Shen P, Zhang Z, Zhu K, Cao H, Liu J, Lu X, Li Y, Jing Y, Yuan X, Fu Y, *et al*: Evodiamine prevents dextran sulfate sodium-induced murine experimental colitis via the regulation of NF-κB and NLRP3 inflammasome. Biomed Pharmacother 110: 786-795, 2019.
20. Cima G: AVMA guidelines for the euthanasia of animal: 2013 Edition. JAVMA J Am Vet Med Assoc 242: 715-716, 2013.
21. Kim JJ, Shajib MS, Manocha MM and Khan WI: Investigating intestinal inflammation in DSS-induced model of IBD. J Vis Exp 60: 3678, 2012.
22. Teng S, Hao J, Bi H, Li C, Zhang Y, Zhang Y, Han W and Wang D: The protection of crocin against ulcerative colitis and colorectal cancer via suppression of NF-κB-mediated inflammation. Front Pharmacol 12: 639458, 2021.
23. Shin HS, Satsu H, Bae MJ, Zhao Z, Ogiwara H, Totsuka M and Shimizu M: Anti-inflammatory effect of chlorogenic acid on the IL-8 production in Caco-2 cells and the dextran sulphate sodium-induced colitis symptoms in C57BL/6 mice. Food Chem 168: 167-175, 2015.
24. Dou B, Hu W, Song M, Lee RJ, Zhang X and Wang D: Anti-inflammation of Erianin in dextran sulphate sodium-induced ulcerative colitis mice model via collaborative regulation of TLR4 and STAT3. Chem Biol Interact 324: 109089, 2020.
25. Ficarro SB, McCleland ML, Stukenberg PT, Burke DJ, Ross MM, Shabanowitz J, Hunt DF and White FM: Phosphoproteome analysis by mass spectrometry and its application to saccharomyces cerevisiae. Nat Biotechnol 20: 301-305, 2002.
26. Zhang Y, Wang J, Wang C, Li Z, Liu X, Zhang J, Lu J and Wang D: Pharmacological Basis for the Use of Evodiamine in Alzheimer's Disease: Antioxidation and Antiapoptosis. Int J Mol Sci 19: 1527, 2018.
27. Lecoq L, Raiola L, Chabot PR, Cyr N, Arseneault G, Legault P and Omichinski JG: Structural characterization of interactions between transactivation domain 1 of the p65 subunit of NF-κB and transcription regulatory factors. Nucleic Acids Res 45: 5564-5576, 2017.
28. Norgan AP, Coffman PK, Kocher JP, Katzmann DJ and Sosa CP: Multilevel parallelization of AutoDock 4.2. J Cheminform 3: 12, 2011.
29. Zhu J, Li X, Zhang S, Ye H, Zhao H, Jin H and Han W: Exploring stereochemical specificity of phosphotriesterase by MM-PBSA and MM-GBSA calculation and steered molecular dynamics simulation. J Biomol Struct Dyn 35: 3140-3151, 2017.
30. Lee TS, Hu Y, Sherborne B, Guo Z and York DM: Toward fast and accurate binding affinity prediction with pmemdGTI: An efficient implementation of GPU-accelerated thermodynamic integration. J Chem Theory Comput 13: 3077-3084, 2017.
31. Hermosilla L, Prampolini G, Calle P, García de la Vega JM, Brancato G and Barone V: Extension of the AMBER force field for nitroxide radicals and combined QM/MM/PCM approach to the accurate determination of EPR parameters of DMPO-H in solution. J Chem Theory Comput 9: 3626-3636, 2013.
32. Zhang Z, Li Y, Shen P, Li S, Lu X, Liu J, Cao Y, Liu B, Fu Y and Zhang N: Administration of geniposide ameliorates dextran sulfate sodium-induced colitis in mice via inhibition of inflammation and mucosal damage. Int Immunopharmacol 49: 168-177, 2017.
33. Cooper HS, Murthy SN, Shah RS and Sedergran DJ: Clinicopathologic study of dextran sulfate sodium experimental murine colitis. Lab Invest 69: 238-249, 1993.
34. He J, Yang A, Zhao X, Liu Y, Liu S and Wang D: Anti-colon cancer activity of water-soluble polysaccharides extracted from Gloeostereum incarnatum via Wnt/β-catenin signaling pathway. Food Sci Hum Wellness 10: 460-470, 2021.
35. Lasry A, Zinger A and Ben-Neriah Y: Inflammatory networks underlying colorectal cancer. Nat Immunol 17: 230-240, 2016.
36. Uttarawichien T, Khumsri W, Suwannalert P, Sibmooh N and Payuhakrit W: Onion peel extract inhibits cancer cell growth and progression through the roles of L1CAM, NF-κB, and angiogenesis in HT-29 colorectal cancer cells. Prev Nutr Food Sci 26: 330-337, 2021.
37. Grivennikov SI, Greten FR and Karin M: Immunity, inflammation, and cancer. Cell 140: 883-899, 2010.
38. Zhu YH, Gu L, Li YJ, Lin X, Shen H, Cui K, Chen L, Zhou F, Zhao Q, Zhang J, *et al*: miR-148a inhibits colitis and colitis-associated tumorigenesis in mice. Cell Death Differ 24: 2199-2209, 2017.
39. Kim HY, Jeon H, Bae CH, Lee Y, Kim H and Kim S: Rumex japonicus Houtt. Alleviates dextran sulfate sodium-induced colitis by protecting tight junctions in mice. Integr Med Res 9: 100398, 2020.

40. Cheng F, Zhang Y, Li Q, Zeng F and Wang K: Inhibition of dextran sodium sulfate-induced experimental colitis in mice by angelica sinensis polysaccharide. J Med Food 23: 584-592, 2020.
41. West NR, McCuaig S, Franchini F and Powrie F: Emerging cytokine networks in colorectal cancer. Nat Rev Immunol 15: 615-629, 2015.
42. Grivennikov S, Karin E, Terzic J, Mucida D, Yu GY, Vallabhapurapu S, Scheller J, Rose-John S, Cheroutre H, Eckmann L and Karin M: IL-6 and Stat3 are required for survival of intestinal epithelial cells and development of colitis-associated cancer. Cancer Cell 15: 103-113, 2009.
43. Nikolaus S and Schreiber S: Treatment of inflammatory bowel disease. Dtsch Med Wochenschr 138: 205-208, 2013.
44. Mitselou A, Grammeniatis V, Varouktsi A, Papadatos SS, Katsanos K and Galani V: Proinflammatory cytokines in irritable bowel syndrome: A comparison with inflammatory bowel disease. Intest Res 18: 115-120, 2020.
45. Han S, Yoon K, Lee K, Kim K, Jang H, Lee NK, Hwang K and Young Lee S: TNF-related weak inducer of apoptosis receptor, a TNF receptor superfamily member, activates NF-kappa B through TNF receptor-associated factors. Biochem Biophys Res Commun 305: 789-796, 2003.
46. Khan MR, Uwada J, Yazawa T, Islam MT, Krug SM, Fromm M, Karaki S, Suzuki Y, Kuwahara A, Yoshiki H, *et al*: Activation of muscarinic cholinoceptor ameliorates tumor necrosis factor-α-induced barrier dysfunction in intestinal epithelial cells. FEBS Lett 589: 3640-3647, 2015.
47. Bruno ME, Rogier EW, Arsenescu RI, Flomenhoft DR, Kurkjian CJ, Ellis GI and Kaetzel CS: Correlation of biomarker expression in colonic mucosa with disease phenotype in crohn's disease and ulcerative colitis. Dig Dis Sci 60: 2976-2984, 2015.
48. Park SY, Ku SK, Lee ES and Kim JA: 1,3-Diphenylpropenone ameliorates TNBS-induced rat colitis through suppression of NF-κB activation and IL-8 induction. Chem Biol Interact 196: 39-49, 2012.
49. Durko Ł, Stasikowska-Kanicka O, Wagrowska-Danilewicz M, Danilewicz M and Malecka-Panas E: Expression of epithelial growth factor receptor, tumor necrosis factor-α and nuclear factor κB in inflammatory bowel diseases. Prz Gastroenterol 8: 262-267, 2013.
50. Tesoriere L, Attanzio A, Allegra M, Gentile C and Livrea MA: Indicaxanthin inhibits NADPH oxidase (NOX)-1 activation and NF-κB-dependent release of inflammatory mediators and prevents the increase of epithelial permeability in IL-1β-exposed Caco-2 cells. Br J Nutr 111: 415-423, 2014.
51. Hundorfean G, Neurath MF and Mudter J: Functional relevance of T helper 17 (Th17) cells and the IL-17 cytokine family in inflammatory bowel disease. Inflamm Bowel Dis 18: 180-186, 2012.
52. De Simone V, Franzè E, Ronchetti G, Colantoni A, Fantini MC, Di Fusco D, Sica GS, Sileri P, MacDonald TT, Pallone F, *et al*: Th17-type cytokines, IL-6 and TNF-α synergistically activate STAT3 and NF-kB to promote colorectal cancer cell growth. Oncogene 34: 3493-3503, 2015.
53. Aranda CJ, Ocón B, Arredondo-Amador M, Suárez MD, Zarzuelo A, Chazin WJ, Martínez-Augustin O and Sánchez de Medina F: Calprotectin protects against experimental colonic inflammation in mice. Br J Pharmacol 175: 3797-3812, 2018.
54. Kwon CH, Moon HJ, Park HJ, Choi JH and Park DY: S100A8 and S100A9 promotes invasion and migration through p38 mitogen-activated protein kinase-dependent NF-κB activation in gastric cancer cells. Mol Cells 35: 226-234, 2013.
55. Luo X, Yue B, Yu Z, Ren Y, Zhang J, Ren J, Wang Z and Dou W: Obacunone protects against ulcerative colitis in mice by modulating gut microbiota, attenuating TLR4/NF-κB signaling cascades, and improving disrupted epithelial barriers. Front Microbiol 11: 497, 2020.
56. Shi YJ, Hu SJ, Zhao QQ, Liu XS, Liu C and Wang H: Toll-like receptor 4 (TLR4) deficiency aggravates dextran sulfate sodium (DSS)-induced intestinal injury by down-regulating IL6, CCL2 and CSF3. Ann Transl Med 7: 713, 2019.
57. Karin M: Nuclear factor-kappaB in cancer development and progression. Nature 441: 431-436, 2006.
58. Han W, Zhu J, Wang S and Xu D: Understanding the phosphorylation mechanism by using quantum chemical calculations and molecular dynamics simulations. J Phys Chem B 121: 3565-3573, 2017.